UNIVERSITY OF TARTU

Faculty of Science and Technology

Institute of Physics

Oskar Tamm

Super-Resolution Correlating Optical Endoscopy

Bachelor's thesis (12 ECTS)

Supervisors: Vijayakumar Anand, Ph.D.

Vipin Tiwari, Ph.D.

Shivasubramanian Gopinath, M.Sc.

Tartu 2024

Abstract

Optical endoscopy is a widely used minimally invasive diagnostic tool for imaging internal organs. The imaging resolution is defined by the numerical aperture of the lens. In this study, we proposed and demonstrated a coded aperture-based Super-resolution Correlating OPtical Endoscopy (SCOPE) system. In SCOPE, modified recording and reconstruction methods are introduced with the existing built-in endoscopy lens as a coded aperture. Instead of recording a single image, multiple images of the object are recorded by scanning the tip of the endoscopy system around the object. The recorded low-resolution images of the object are arranged as sub-matrices in a 2D matrix. Another similar 2D matrix with either recorded or synthesized Point Spread Functions (PSFs) is created. The 2D matrices of the object and the PSF were processed using a deconvolution algorithm to reconstruct the super-resolution image of the object. Both simulation and proof-of-concept experimental studies have been presented. SCOPE neither requires any additional optical element nor any changes in the endoscopy system itself and therefore can be implemented easily in commercial endoscopy systems.

Keywords: Indirect imaging, coded aperture correlation holography, endoscopy, microscopy, imaging and super-resolution.

CERCS: T121 – Signal processing

Ülilahutusega seostatud optiline endoskoopia

Lühikokkuvõte:

Optiline endoskoopia on laialt levinud, mitteinvasiivne diagnostika meetod organite uurimiseks. Endoskoobi nurklahutusvõime defineerib tema läätse numbriline ava. Antud töös näidati kodeeritud aval põhinevat ülilahutusega seostatud optilise endoskoopia süsteemi (SCOPE). SCOPE-s on kodeeritud avaks endoskoobi lääts ning kasutatakse muudetud lindistusmeetodit. Selle asemel, et teha üks pilt, tehakse uuritavast objektist mitu pilti, muutes endoskoobi otsa asendit iga võtte järel. Saadud pildid paigutatakse alammaatriksitena 2D maatriksisse. Luuakse teine identne maatriks koos lindistatud või sünteesitud punktkostefunktsioonidega. Maatrikseid kasutatakse dekonvolutsiooni algoritmis, et saada parema lahutusvõimega pilt objektist (ülilahutus). Töös esitletakse nii simulatsiooni, kui ka

katse tulemused. SCOPE-i kasutamine ei nõua lisanduvaid optilisi elemente ega teisi muudatusi endoskoobi ehitusele ning seetõttu on seda lihtne kasutusele võtta juba loodud endoskoopides.

Märksõnad: kaudne pildindus, kodeeritud avaga seoseholograafia, endoskoopia, mikroskoopia, pildindus ja ülilahutusvõime

CERCS: T121 – Signaalitöötlus

Contents

1. Introduction

Endoscopy is a versatile tool of a modern-day physician for imaging and surgery in internal organs [1]. Like most commercial imaging systems, endoscopy uses a direct mode of imaging for recording an object [2, 3]. In direct imaging mode, the light from the object is collected and focused by a refractive lens on an image sensor or the eye with the image formation governed by the conventional laws of optics [4]. The lateral resolution of imaging is given as $\sim\lambda/NA$, where NA is the numerical aperture given as $D/2u$, where D is the diameter of the lens and u is the distance between the object and the lens. In the case of a single lens imaging system $u = \left(\frac{1}{f} - \frac{1}{v}\right)^{-1}$, where f is the lens focal length, and v is the distance between the detection plane and the lens. Considering the necessity for the distal tips of endoscopes to have a small diameter to probe as many different areas of the human body as possible, there is a clear conflict between surgical interests, and imaging techniques. In recent years, there have been some attempts to push endoscopy technology beyond the conventional imaging framework [5-10]. In most commercial endoscopic systems, the light source and image sensor are part of the probing unit entering the body. The sample is illuminated by the light source and directly recorded by the image sensor with an integrated lens system. The recorded signal is transmitted as an electronic signal to the computer through electrical cables. In [9,10], an ultrathin endoscopy system has been realized by moving the image sensor and light source out of the probing unit. Since the object information is transferred through optical fiber, the image of the object can be obtained only after a computational processing of the recorded distributions. In [9] and [10], deep learning and computational algorithms have been used respectively to obtain the object information. While the above developments will enable moving beyond the state-of-the-art of modern-day endoscopic systems, implementing them requires fundamental changes to the existing endoscope architecture which may be a burden on the industry without evidence of substantial improvements.

In recent years, Interferenceless Coded Aperture Correlation Holography (I-COACH), a new sub-field of imaging, has been growing rapidly and is emerging as a technology for the future [11]. The I-COACH imaging technique is an indirect imaging technique consisting of at least two steps: optical recording and computational reconstruction. In the optical recording step, instead of the image of an object, a distorted projection of the object is recorded. In the computational reconstruction step, the image of the object is reconstructed with additional

information that cannot be obtained through direct imaging mode. Many imaging techniques developed based on the foundations of I-COACH have capabilities beyond the conventional limits in several imaging dimensions, resolution, field of view, etc. They are thoroughly reviewed in [12-14].

In this research project, we propose and demonstrate a Super-resolution Correlating OPtical Endoscopy (SCOPE) system based on I-COACH and the understanding gained from recent implementations [15-17]. In SCOPE, multiple recordings of an object are made using a regular endoscopy system by scanning the tip of the endoscope around the object. The recorded images are arranged in a 2D matrix and processed with an identical matrix consisting of the recordings of a point using a deconvolution algorithm [18]. The reconstructed image has an improved resolution compared to the individual recording with a higher signal-to-noise ratio. This approach does not require fundamental changes in the architecture of the endoscopy system like that of [9,10,15] and therefore can be easily implemented with existing commercial endoscopy systems.

The thesis consists of seven sections. In the next section, an overview of endoscopy and computational imaging concepts are presented. Then the methodology of SCOPE is discussed in the third section. The simulation studies are presented in the fourth section. Proof-of-concept experimental studies are presented in the fifth section. The results and the pathway for implementing SCOPE in the existing commercial endoscopy system are discussed in the sixth section. The conclusion and future perspectives are presented in the final section.

2. Theoretical background

2.1 Endoscopy

Endoscopy is a minimally invasive diagnostic technique for imaging and surgery in internal organs. The first modern endoscope was invented by Dr Philipp Bozzini in 1805, which he called the Lichtleiter (light conductor). Though his invention was ingenious, politics at the time had prevented wider usage of Bozzinis' invention. As technology developed, so did endoscopy. New inventions like incandescent bulbs, fiber optics, CCD-s were all used to improve endoscopy technology [19].

The first endoscopic procedures were used to inspect the urethra, the bladder, and the vagina [19]. Today endoscopy has grown into a wide-ranging surgical tool that is used to examine almost the whole body. A thorough list of different types of endoscopies is shown in TABLE 1 [20].

Commercial endoscopes are sophisticated with many variations and options depending upon the required application. They consist of a handle and a thin flexible tube. The handle has a control system, usually control wheels or handles, to control the angle of the distal tip. Many endoscopes also have a biopsy inlet to extract tissue samples or remove foreign objects. The length of the flexible tube can vary from a few centimetres to a few meters and its diameter can vary from a few millimetres to two centimetres, depending on the object being examined. The distal tip of an endoscope has LED lights, and an optical system for imaging, and often a channel connected to the biopsy inlet. [19]

Type	Area examined	Where scope is inserted
Arthroscopy	Joints	Through a small incision near the examined joint
Bronchoscopy	Lungs	Into the nose or mouth
Colonoscopy	Colon	Through the anus
Cystoscopy	Bladder	Through the urethra
Enteroscopy	Small intestine	Through the mouth or anus
Hysteroscopy	Inside of the uterus	Through the vagina
Laparoscopy	Abdominal or pelvic area	Through a small incision near the examined area
Laryngoscopy	Larynx	Through the mouth or nostril
Mediastinoscopy	The area between the lungs	Incision above the breastbone
Sigmoidoscopy	Rectum and lower part of the large intestine (sigmoid colon)	Into the anus
Thorascopy (pleuroscopy)	Area between the lungs and the chest wall	Through a small incision in the chest
Esophagogastroduodenoscopy	Esophagus and upper intestinal tract	Through the mouth
Ureteroscopy	Ureter	Through the urethra

TABLE 1: A list of endoscopic procedures, what area is examined, and an endoscope is transported to the right area.

2.2 Computational imaging

Computational imaging is an emerging domain of optics and photonics, which encompasses the development of novel imaging modalities in the framework of robust optical design followed by advanced computational algorithms. Computational imaging is used to obtain enhanced imaging characteristics (resolution, Depth of Field (DOF), Signal to Noise Ratio (SNR)), either in the pre-recording or post-recording processes. In general, conventional imaging is direct – images are recorded directly by a camera. Computational imaging uses an

indirect imaging mode. Indirect imaging is a process where a modified version of an object's information is recorded and the image of the object is reconstructed using suitable computational reconstruction algorithms. One prominent indirect imaging method is coded aperture imaging, which was originally proposed for X-ray imaging [21] and later used also for imaging using visible light. Recently, the two different concepts - coded aperture imaging and incoherent digital holography were combined into a new indirect imaging method, Coded Aperture Correlation Holography (COACH) [22]. COACH was proposed as a generalized case of Fresnel Incoherent Correlation Holography (FINCH) which is a well-known technique of recording holograms based on the concept of self-interference [23]. Further developments in COACH led to the more efficient technique, I-COACH, which can demonstrate 3D imaging without interference between two waves [11]. Multiple developments in the I-COACH technique, such as aperture engineering and reconstruction methods, have been demonstrated in the recent past [12]. Some examples of reconstruction algorithms developed for I-COACH are: Non-Linear Reconstruction (NLR), Lucy-Richardson Algorithm (LRA), and Lucy-Richardson-Rosen Algorithm (LRRA), which is an algorithm that combines the first two.

An interesting application for COACH is incoherent imaging with Synthetic Aperture (SA). SA is a conventional super-resolution technique to accomplish image resolution beyond the diffraction limit, which is governed by the Numerical Aperture (NA) of a lens. The incoherent SA imaging is usually realized by at least two optical channels operating simultaneously. The Object Response Intensity (ORI) and Point Spread Function (PSF) are recorded over time from several viewpoints within the SA region and processed to reconstruct an image of the object with a resolution equivalent to complete SA. Recently, a super-resolution endoscopy system based on I-COACH was reported [15] that used a modified endoscope configuration with a ring-shaped coded aperture.

In this study, a Super-resolution Correlating OPtical Endoscopy (SCOPE) system is proposed and experimentally demonstrated. SCOPE works on the principle of I-COACH and leverages noise averaging from multiple recordings around the object to achieve a super-resolution.

3. Methodology

The optical configuration of SCOPE for recording and computational reconstruction is shown in FIGURE 1(a). The imaging unit consists of an illumination source, a lens, and an image sensor. An object is recorded and a point object is optionally recorded. The PSF can be obtained by either recording, extracted from the object's response intensity or synthesized depending upon the restrictions around the sample. In this study, the PSF was optically recorded. The imaging procedure involves multiple recordings of a point object and an object itself by scanning the tip of the endoscope around the object. The recorded object intensity and PSFs are arranged as sub-matrices in a large matrix and processed using one of the deconvolution methods discussed in [18]. The computational reconstruction generates an image with a lateral resolution higher than that of the directly recorded image and the reconstructed image with a single recording using a deconvolution algorithm as shown in FIGURE 1(b). In this study, only spatially incoherent illumination is considered as mostly such light sources are used in commercial endoscopy systems. A free space optical configuration with object and image distances z_s and z_h and a lens with a focal length f mimicking SCOPE is shown in FIGURE 2 which is used experimental demonstration.

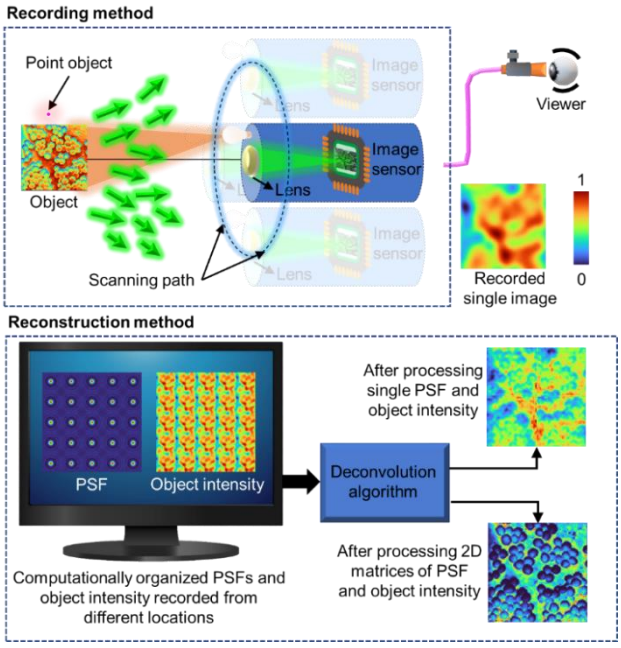

FIGURE 1. (a) Optical recording configuration of SCOPE.
(b) Computational reconstruction configuration of SCOPE.

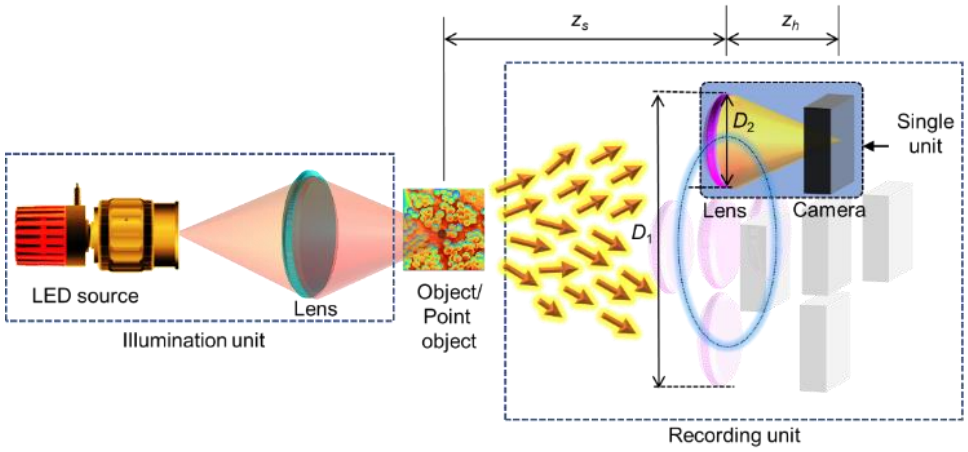

FIGURE 2. Free space optical configuration for mimicking SCOPE.

The resolution improvement is achieved due to the deconvolution, first at the level of a single recording [24] and then at the level of the array of multiple recordings. The deconvolution process of the LRRA [16, 17, 25] used herein magnifies the high frequencies inside the spectral bandwidth. Therefore, because the fine details of an object are represented mostly in the high frequencies of the spatial spectrum, the image resolution is enhanced, but the noise is also magnified. If the noise has a zero mean, multiple independent deconvolution events can reduce the noise. Multiple recordings at different times guarantee multiple independent events of detection noise added to the recorded images.

The deconvolution algorithm used in this study, LRRA, is shown in FIGURE 3. LRRA is an iterative algorithm, meaning that the steps of the algorithm are repeated until an optimal solution is obtained. The first solution is the object response intensity. This solution is convolved with the PSF. A ratio of the solution and its convolution is correlated using NLR. Finally, the resulting “residue” is multiplied by the last solution. The ORI distribution will look more like the actual object intensity distribution after each iteration.

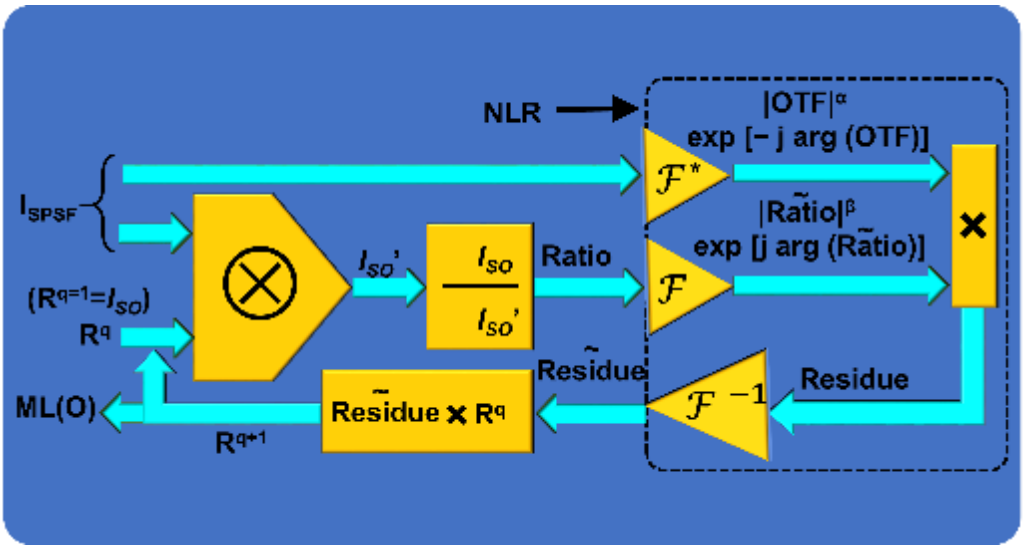

FIGURE 3. Schematic of the Lucy–Richardson–Rosen algorithm. OTF – optical transfer function; q—number of iterations of LRRA; ⊗—2D convolutional operator; R^q is the qth solution; and q is an integer; when $q = 1$, $R^q = I_O$; and α and β are varied from −1 to 1; ~ - Fourier Transform, * complex conjugate; NLR is a nonlinear reconstruction; $\mathcal{F}$ and $\mathcal{F}^{-1}$ are Fourier and inverse Fourier transforms, respectively.

4. Simulation studies

A computer simulation was carried out in MATLAB with a matrix size of 500 × 500 pixels, pixel size $\Delta = 10$ μm, wavelength $\lambda = 650$ nm. A sub-matrix window with a size of 100 × 100 pixels was used for scanning over the 500 × 500 pixels matrix with a step size of 100 pixels. The object and image distances were set as $z_s = 80$ cm and $z_h = 26.7$ cm to satisfy the imaging condition for a lens of focal length $f = 20$ cm. Fresnel propagators have been used to verify the idea and therefore the distances are larger. However, by changing Δ, λ and distances, the simulation results can be scaled to different distances and wavelengths respectively.

At first, a binary USAF object image was used as the test object for the simulation studies as shown in FIGURE 4(a). The test object was downsized to a reduced number of pixels for simulation which is shown in FIGURE 4(b). A total of 9 recordings in a 3-by-3 configuration were simulated from the I_{PSF} and I_O. The images of the accumulated phase function of the lens, $I_{SPSF,}$ and I_{SO} are shown in FIGUREs 4(c)-4(e) respectively. The magnified single recording, reconstruction by processing I_{PSF} and I_O and reconstruction by processing I_{SPSF} and I_{SO} are shown in FIGUREs 4(f)-4(h) respectively [25]. The line plots (lateral profiles) of the Region Of Interest (ROI) in FIGUREs 4 (b)-4(h) are shown in FIGURE 4(i).

In the next step, SCOPE was simulated for a grayscale test object (a neuron image) and a downsized test object, as shown in FIGUREs 4(j) and 4(k) respectively. In this case, the object and image distances were set as $z_s = 100$ cm and $z_h = 11.11$ cm to satisfy the imaging equation for a lens with a focal length $f = 10$ cm. A total of 25 recordings arranged in a 5×5 configuration were simulated for the I_{PSF} and I_O. Images of the accumulated phase functions of the lens, I_{SPSF} and I_{SO} are shown in FIGUREs 4(l)-4(n), respectively. The magnified single recording, reconstruction by processing I_{PSF} and I_O and reconstruction by processing I_{SPSF} and I_{SO} are shown in FIGUREs 4(o)-4(q), respectively. The line plot (lateral profile) of the ROIs in FIGUREs 4(k)-4(q) are shown in FIGURE 4(r). The LRRA was operated with the following conditions ($\alpha = 0$, $0.5 \leq \beta \leq 0.7$, $4 \leq n \leq 7$), where n is the number of iterations. As seen from the simulation results, with SCOPE, the image resolution can be significantly improved, and the improvement is proportional to the number of recordings.

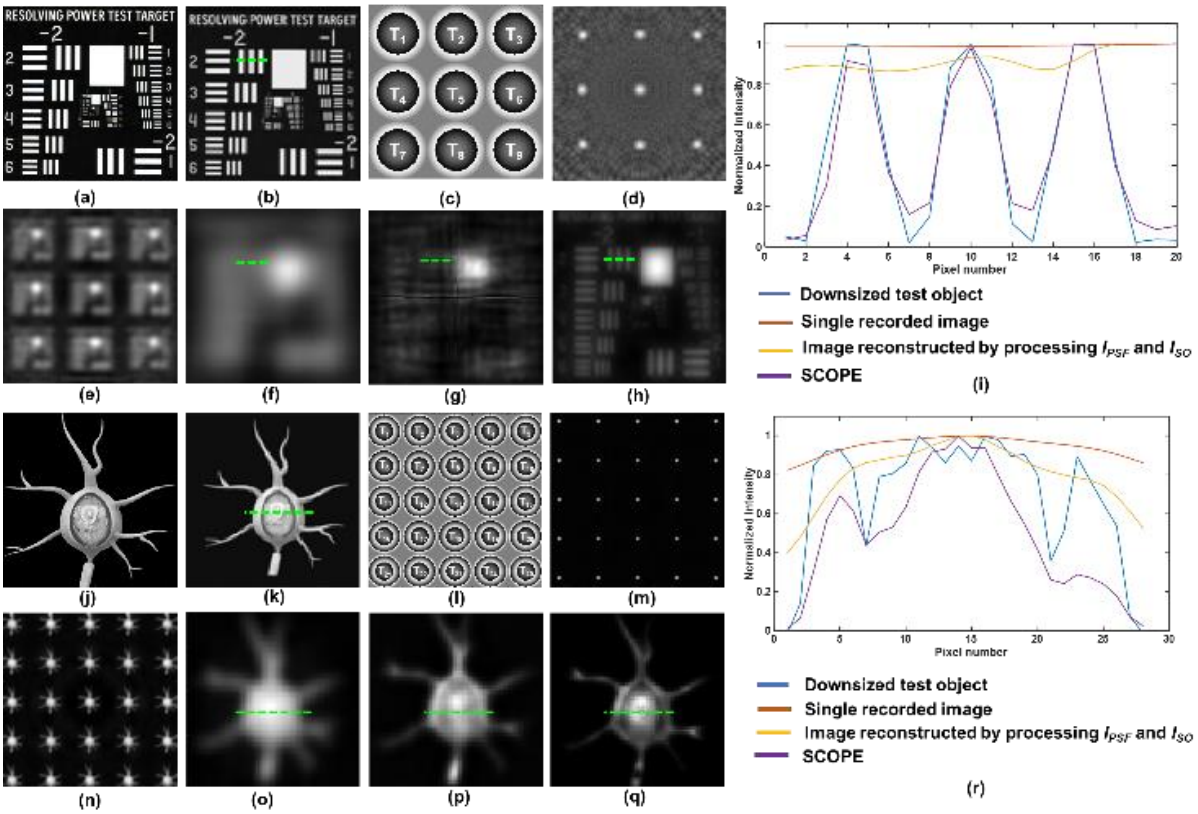

FIGURE 4. Simulation results: (a) Binary test object. (b) Downsized binary test object. (c) Accumulated phase obtained by scanning the lens and camera unit at T_1 to T_9. (d) I_{SPSF}, (e) I_{SO}, (f) single recorded image, and (g) image reconstructed by processing I_{PSF} and I_{SO}. (h) SCOPE reconstruction, (i) line plot (lateral profile) for the region of interest (ROI) for FIGURE 4 (b, f, g, h) (the green dashed line shows the data extraction location of the line plot). (j) Grayscale test object. (k) Downsized grayscale test object. (l) Accumulated phase obtained by scanning the lens and camera unit at T_1 to T_{25}. (m) I_{SPSF}, (n) I_{SO}, (o) single recorded image, and (p) image reconstructed by processing I_{PSF} and I_{SO}. (q) SCOPE reconstruction and (r) line plot (lateral profile) for the ROI in FIGURE 4 (k, o, p, q) (the green dashed line shows the data extraction location of the line plot).

5. Experiments

FIGURE 5(a) illustrates the schematic of the experimental configuration of SCOPE and a photograph of experimental setup is shown in FIGURE 5(b). A red-light beam, emanating from a high-power LED (Thorlabs, 940 mW, λ = 660 nm and $\Delta\lambda$ = 20 nm, Newton, MA, USA) is collimated by a refractive lens (L1) of focal length 50 mm. An iris1, and a diffuser (D) (Thorlabs Ø1" Ground Glass Diffuser-220 GRIT, Newton, MA, USA) are used to control the initial beam illumination and to remove the grating lines of the LED, respectively. This collimated beam is passed through a linear polarizer (P), oriented along the active axis of SLM. An object is critically illuminated using a converging lens (L2) of focal length 50 mm. Light from the object is then collected by a collimating lens (L3) of focal length 50 mm and an iris2. The collimated beam was incident on an SLM (Thorlabs Exulus HD2, 1920 × 1200, pixel size = 8 µm, Newton, MA, USA) through a beam splitter (BS). Light reflected from SLM is directed to an image sensor (Zelux CS165MU/M 1.6 MP monochrome CMOS camera, 1440 × 1080 pixels with pixel size ~3.5 µm, Newton, MA, USA), which is placed at the reflecting arm of BS at a distance of 178 mm from SLM.

In the experiment, a pinhole of diameter 25 µm was used to record the I_{PSF} with the image sensor. Three different objects were used as I_O: O1 – two points (25 µm diameter each, 20 µm apart), O2 – two gratings (horizontal and vertical) with digit 4 from Group 4 of R1DS1N—Negative 1951 USAF Test Target, Ø1"), and O3 – insect wing.

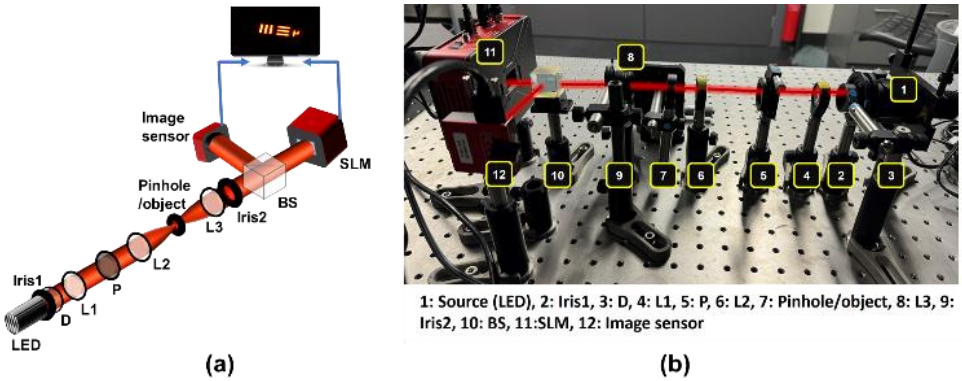

FIGURE 5. Experimental configuration of SCOPE (a) schematic of experimental setup (b) photograph of experimental setup. [LED: Light Emitting Diode, D: Diffuser, Ln (n=1,2,3): Lens, BS: Beam Splitter, SLM: Spatial Light Modulator].

As the first step, SCOPE was tested for the simple object O1, i.e., two points (each with a size of 25 µm and a distance of 20 µm). Lens Array Mask (LAM) for SCOPE was designed by combining subapertures (55 SLM pixel radius each) in a regular 3-by-3 array. The PSF and the corresponding Object Response Intensities (ORIs) were recorded. In addition, the PSF and ORI were also recorded for a Diffractive Lens Mask (DLM) with a focal length of 178 mm with a Combined Aperture Mask (CAM), which is a DLM but with the same aperture size as the LAM. FIGURE 6(a-d) shows the (a) CAM (3×3), (b) LAM (3×3), (c) recorded PSF for the LAM, and (d) ORI for the LAM. The recorded direct images for the CAM (DICAM) and ORI for a single element of the LAM in the role of regular endoscopy are presented in FIGUREs 6(e, f), respectively. The reconstruction results for regular endoscope imaging and SCOPE for O1 using LRRA are depicted in FIGURE 6(g, h). For visibility comparison, a line plot is shown for the highlighted region of FIGURE 6(e-h) in FIGURE 6(i). A comparison of FIGUREs 6(e-h) shows that two points are best resolved for SCOPE. Furthermore, the full width at half maximum (FWHM) was calculated from the plots in FIGURE 6 (i) and is shown in FIGURE 6 (j). The minimum value of the FWHM was obtained in SCOPE compared to the other methods, which demonstrates enhanced resolution.

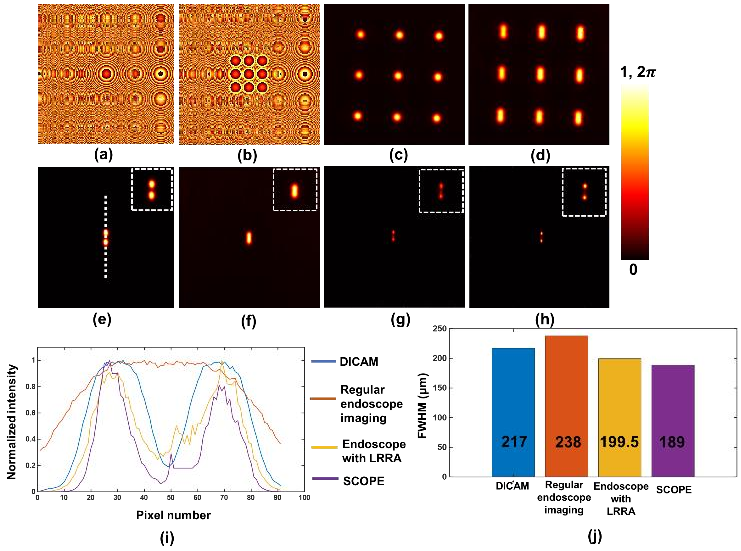

FIGURE 6. Experimental results for Object1 (O1). (a) CAM (3×3), (b) LAM (3×3), (c) recorded PSF using LAM, (d) recorded ORI using LAM, (e) ORI using CAM, (f) ORI for regular endoscope, (g) regular endoscope using LRRA, (h) SCOPE using LRRA, (i) Line plot for region of interest (ROI), (white dashed line shows data extraction location for line plot), (j) FWHM plot corresponding to FIGURE 6 (i). CAM: combined aperture mask, LAM: lens array mask, DICAM: direct imaging with combined aperture mask, LRRA: Lucy-Richardson-Rosen algorithm, ORI: object response intensity, SCOPE: super-resolution correlating optical endoscopy, FWHM: full-width half maximum.

In the next experiment, the feasibility of SCOPE was tested for multi-element object O2 (Group 4 elements of R1DS1N—Negative 1951 USAF Test Target, Ø1"). Similarly, the PSFs and ORIs were recorded for O2. In this case, the LAM for SCOPE was designed by combining 16 sub-apertures (55 SLM pixels each) in a regular 4-by-4 array. FIGURE 7(a-d) shows the (a) CAM (4×4), (b) LAM (4×4), (c) recorded PSF for the LAM, and (d) ORI for the LAM. The recorded ORIs for the CAM and ORI for direct recording as regular endoscopy are presented in FIGUREs 7(e, f), respectively. The reconstruction results for regular endoscope imaging and SCOPE for O2 using LRRA are depicted in FIGURE 7(g, h). On comparing FIGUREs 7(e-h), all three elements (vertical, horizontal gratings, digit 4) are best resolved in the case of SCOPE. Furthermore, the line plot shown in FIGURE 7(i) along the vertical grating of the highlighted region confirms the resolution enhancement for SCOPE compared to direct endoscope recording. Furthermore, the FWHM was calculated from the plots in FIGURE 7 (i) and is shown in FIGURE 7 (j). The minimum value of the FWHM was obtained in SCOPE compared to the other methods for O2.

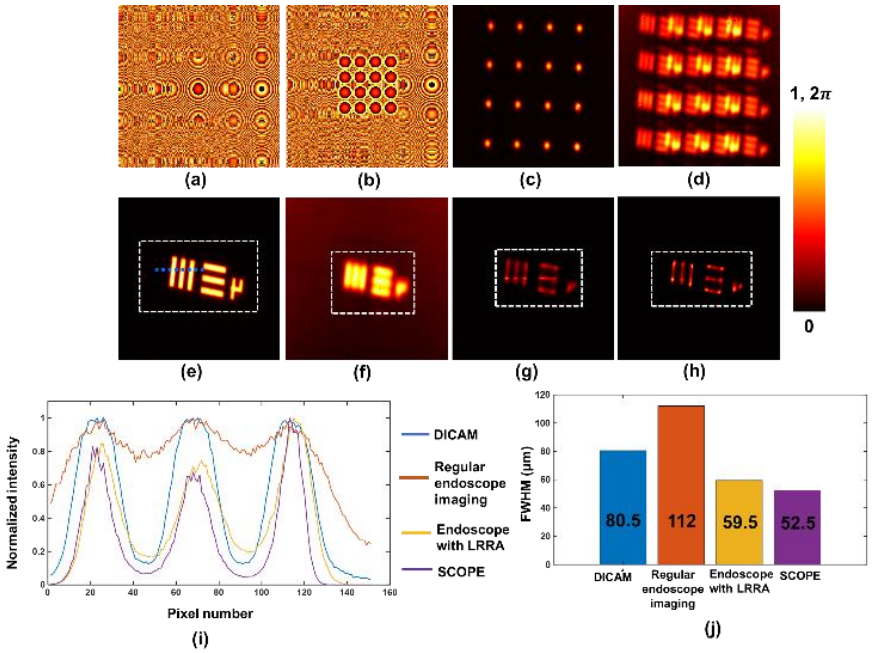

FIGURE 7. Experimental results for multielement object (O2). (a) CAM (4×4), (b) LAM (4×4), (c) recorded PSF using LAM, (d) recorded ORI using LAM, (d) ORI using CAM, (f) ORI for regular endoscope, (g) regular endoscopy using LRRA, (h) SCOPE using LRRA, (i) Line plot for Region of Interest (ROI), (blue dashed line shows data extraction location for line plot), (j) FWHM plot corresponding to FIGURE 7 (i), CAM: Combined Aperture Mask, LAM: Lens Array Mask, DICAM: Direct Imaging with Combined Aperture Mask, LRRA: Lucy-Richardson-Rosen Algorithm, ORI: Object Response Intensity, SCOPE: Super-resolution Correlating Optical Endoscopy, FWHM: Full-Width Half Maximum).

Finally, SCOPE was implemented for O3, i.e., a biological sample (insect wing). We recorded PSFs and ORIs for O3 similar to those for O1 and O2, and the corresponding results are shown in FIGURE 8. FIGURE 8(a-d) shows the (a) CAM (3×3), (b) LAM (3×3), (c) recorded PSF for the LAM, and (d) ORI for the LAM. The recorded ORIs for the CAM and ORI for direct recording as regular endoscopy are presented in FIGURE 8(e, f), respectively. The reconstruction results for regular endoscope imaging and SCOPE for O3 using LRRA are depicted in FIGURE 8(g, h). A comparative analysis of FIGURE 8(e-h) shows enhanced spatial features of O3 using SCOPE compared to direct endoscope recording. A line plot for the ROI (along the blue dashed line) for FIGURE 8(e-h) is shown in FIGURE 8(i) to indicate the resolution enhancement of O3 using SCOPE. For this entire experimental study, LRRA was performed under the following conditions (α = 0.4, β =1, $40 \leq n \leq 55$), where n is the number of iterations.

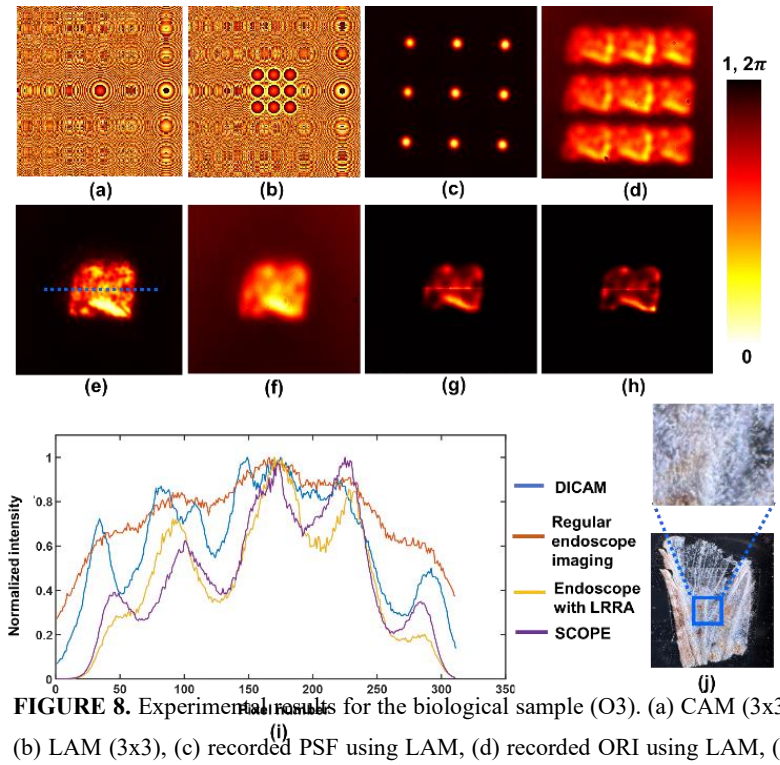

FIGURE 8. Experimental results for the biological sample (O3). (a) CAM (3x3), (b) LAM (3x3), (c) recorded PSF using LAM, (d) recorded ORI using LAM, (d) ORI using CAM, (f) ORI for regular endoscopy, (g) regular endoscopy using LRRA, (h) SCOPE using LRRA, (i) Line plot for Region of Interest (ROI), (blue dashed line shows data extraction location for line plot), (j) Actual photograph of biological sample (blue box represents the ROI and magnified version of ROI is shown in its top). CAM: combined aperture mask, LAM: lens array mask, DICAM: direct imaging with combined aperture mask, LRRA: Lucy-Richardson-Rosen algorithm, ORI: object response intensity, SCOPE: super-resolution correlating optical endoscopy.

6. Discussion

SCOPE has been developed to improve the resolution limit of commercial endoscopes without the need to rework their architecture. The preliminary results are promising, although implementing SCOPE in a real system does present some additional challenges.

Commercial endoscopes can have a prominent fisheye effect, which can cause issues with the reconstruction. Especially if the PSF doesn't account for the effect. The fisheye effect however, can be lessened or even eliminated before starting image reconstruction.

In general, the doctor manoeuvres the endoscope through the human body using an angulation controller that has wires that are connected to the tip of the endoscope [26]. When the angulation controller is adjusted, the wires are pulled causing a turn in the tip of the endoscopic system. Most of the commercial endoscopic systems consists of *x*-*y* controls that allows the doctor to manoeuvre the distal tip of an endoscope along different directions to follow through the turns of the gastrointestinal tract.

Conventional manoeuvring causes an additional linear phase in the spatial spectrum. This linear phase is important as it shifts the image in the image sensor. However, this shift does not affect the reconstruction results, if the PSF experiences an identical shift.

An ideal scenario would be that the doctor clicks the SCOPE recording function and the tip of the endoscope moves to predefined locations without tilt acquiring multiple images of the object and the recordings are processed in the computer real-time and the reconstruction result is shown to the doctor.

7. Conclusion

In this research project, a Super-resolution Correlating OPtical Endoscopy (SCOPE) system is proposed and demonstrated with both simulation studies as well as proof-of-concept experiments. SCOPE is based on the principle of I-COACH and involves noise averaging to achieve super-resolution. Enhanced resolution can be achieved by imaging the object at multiple locations. Enhanced resolution can be achieved by imaging an object over time at multiple locations around the object. In SCOPE, image arrays of sizes (3×3) and (4×4) of objects (O1, O2, and O3) were recorded using LAM, processed with an identical PSF array, and reconstructed using the LRRA algorithm. The reconstruction results demonstrate an enhanced resolution for SCOPE compared to individual recording. We believe that the developed technique can be quickly absorbed into commercial endoscopy systems to achieve super-resolution imaging.

Publications

O. Tamm, V. Tiwari, S. Gopinath, A. S. J. F. Rajeswary, S. A. Singh, J. Rosen, V. Anand, “Super-Resolution Correlating Optical Endoscopy”, ***IEEE Access*** (accepted for publication 19.05.2024)

O. Tamm, V. Tiwari, S. Gopinath, A.S.J.F. Rajeswary, S. A. Singh, J. Rosen, V. Anand, “Synthetic-Aperture Coded Optical Endoscopy”, ***IEEE International Conference in Image Processing (ICIP),*** (under review).

Acknowledgements

First, and foremost I would like to thank my supervisors, Prof. Vijayakumar Anand, Vipin Tiwari, and Shivasubramanian Gopinath. They were very supportive and extremely helpful at every obstacle. Furthermore, I would like to extend my gratitude to Aravind Simon John Francis Rajesway, Scott Arockia Singh, and Prof. Joseph Rosen for their valuable contribution in discussions, and expertise. Finally, I'm also extremely grateful to my course mates and friends, whose help and support have got me to where I am today.

Oskar Tamm

References

[1] Y. Tang, S. Anandasabapathy, and R. Richards-Kortum, "*Advances in optical gastrointestinal endoscopy: a technical review*," Molecular Oncology, vol. 15, no. 10, pp. 2580–2599, (Sep. 2020).

[2] H.J. Trussell and M. J. Vrhel, "*Fundamentals of Digital Imaging*," (Cambridge: Cambridge University Press, 2008).

[3] P. Suetens, "*Fundamentals of Medical Imaging*," 2nd ed. (Cambridge: Cambridge University Press, 2009).

[4] E. Hecht, "*Optics*," (Pearson Education India, 2012).

[5] L. FU and M. GU, "Fibre-optic nonlinear optical microscopy and endoscopy," *Journal of Microscopy*, vol. 226, no. 3, pp. 195–206, (June. 2007).

[6] M. J. Gora, M. J. Suter, G. J. Tearney, and X. Li, "Endoscopic optical coherence tomography: technologies and clinical applications [Invited]," *Biomedical Optics Express*, vol. 8, no. 5, p. 2405, (Apr. 2017).

[7] L. R. Fisher and W. L. Hasler, "New vision in video capsule endoscopy: current status and future directions," *Nature Reviews Gastroenterology & Hepatology*, vol. 9, no. 7, pp. 392–405, (May 2012).

[8] B. A. Flusberg, E. D. Cocker, W. Piyawattanametha, J. C. Jung, E. L. M. Cheung, and M. J. Schnitzer, "Fiber-optic fluorescence imaging," *Nature Methods*, vol. 2, no. 12, pp. 941–950, (Nov. 2005).

[9] P. Caramazza, O. Moran, R. Murray-Smith, and D. Faccio, "Transmission of natural scene images through a multimode fibre," *Nature Communications*, vol. 10, no. 1, (May 2019).

[10] W. Choi *et al.,* "Flexible-type ultrathin holographic endoscope for microscopic imaging of unstained biological tissues," *Nature Communications*, vol. 13, no. 1, (Aug. 2022).

[11] V. Anand and J. Rosen, "Interferenceless coded aperture correlation holography–a new technique for recording incoherent digital holograms without two-wave interference," *Optics Express*, vol. 25, no. 12, pp. 13883–13896, (June 2017).

[12] J. Rosen *et al.,* "Recent advances in self-interference incoherent digital holography," *Advances in Optics and Photonics*, vol. 11, no. 1, pp. 1–66, Feb. 2019.

[13] J. Rosen, V. Anand, and N. Hai, *Digital holography based on aperture engineering*, (SPIE Press, 2023).

[14] J. Rosen and V. Anand, "Optical Imaging Using Coded Aperture Correlation Holography (COACH) with PSF of Spatial-Structured Longitudinal Light Beams—A Study Review," *Photonics*, vol. 11, no. 2, p. 115, (Feb. 2024).

[15] N. Dubey, J. Rosen, and I. Gannot, "High-resolution imaging system with an annular aperture of coded phase masks for endoscopic applications," *Optics Express*, vol. 28, no. 10, pp. 15122–15137, (May 2020).

[16] Jayavel *et al.,* "Improved Classification of Blurred Images with Deep-Learning Networks Using Lucy-Richardson-Rosen Algorithm," *Photonics*, vol. 10, no. 4, p. 396, (Apr. 2023).

[17] P. A. Praveen *et al.,* "Deep Deconvolution of Object Information Modulated by a Refractive Lens Using Lucy-Richardson-Rosen Algorithm," *Photonics*, vol. 9, no. 9, pp. 625, (Sep. 2022).

[18] J. Rosen and V. Anand, "Incoherent nonlinear deconvolution using an iterative algorithm for recovering limited-support images from blurred digital photographs," *Optics Express*, vol. 32, no. 1, pp. 1034–1046, (Dec. 2023).

[19] Davis CJ and Filipi CJ, "A history of endoscopic surgery" *in Principles of Laparoscopic Surgery Basic and Advanced Techniques*, pp. 3-20 (Springer, New York 1995).

[20] B. Krans, "What Is an Endoscopy," www.healthline.com/health/endoscopy#followup

[21] J. G. Ables, "Fourier Transform Photography: A New Method for X-Ray Astronomy," *Publications of the Astronomical Society of Australia*, vol. 1, no. 4, pp. 172–173, (1968). doi:10.1017/S1323358000011292

[22] Vijayakumar, Y. Kashter, R. Kelner, and J. Rosen, "Coded aperture correlation holography–a new type of incoherent digital holograms," *Optics Express* 24, pp. 12430-12441 (2016).

[23] J. Rosen and G. Brooker, "Digital spatially incoherent Fresnel holography," *Optics Letters*, 32, pp. 912-914, (2007).

[24] W. Zhao, S. Zhao, L. Li, et al. "Sparse deconvolution improves the resolution of live-cell super-resolution fluorescence microscopy," *Nature Biotechnolgy*, vol.40, pp. 606–617 (2022).

[25] V. Anand *et al.*, "Single-shot mid-infrared incoherent holography using Lucy-Richardson-Rosen algorithm," *Opto-Electronic Science*, vol. 1, no. 3, pp. 210006-1–210006-8, (Jan. 2022).

[26] E. Rozeboom *et al.*, "Intuitive user interfaces increase efficiency in endoscope tip control". *Surgical endoscopy, 28*, pp.2600-2605, (Mar. 2014).

Appendices

Appendix 1: MATLAB code for Lucy-Richardson-Rosen Algorithm (Commented version)

%% Loading the PSF image

A=double(imread('File location')); *%Read the image file of PSF and convert it into double precision arrays*

A=A(:,:,1); *%Extract the channel of interest - RGB, A(:,:,1) extracts Red A(:,:,2) extracts Green and A(:,:,3) extracts Blue*

A=A/max(max(A)); % *Normalise the matrix between 0 and 1*

imagesc(A) *% Display image*

%% Loading the object intensity distribution image

B=double(imread('File location')); *%Read the image file of object intensity distribution and convert it into double precision arrays*

B=B(:,:,1); *%Extract the channel of interest - RGB, A(:,:,1) extracts Red A(:,:,2) extracts Green and A(:,:,3) extracts Blue*

B=B/max(max(B)); *% Normalise the matrix between 0 and 1*

figure; imagesc(B) *% Display image*

%% Performing Lucy-Richardson-Rosen Algorithm

PSF=A; *% Assign A to PSF*

OI=B; % *Assign B to Object intensity distribution*

S1 = OI; *% Initial guess solution is set as the object intensity pattern*

OTF = psf2otf(PSF,size(OI)); *% Convert PSF to OTF*

iterations = 10; *% Enter the iteration number – for example start with 5*

figure;colormap turbo *% Open new FIGURE and set colormap turbo*

for i=1:iterations *%start for loop*

i % *show iteration number*

FC = (ifft2(fft2(S1).*OTF)); *% Forward Convolution*

```
    ratio = OI./FC; % Calculate ratio

    ratio_f = fft2(ratio); % Fourier transform of ratio

    alpha = 0.4; % Enter alpha value between 0 and 1; when alpha is 1 and beta is 1, it is Lucy-Richardson Algorithm

    beta = 1; % Enter beta value between 0 and 1

    residue = ifft2(conj((abs(OTF).^alpha).*exp(1i*angle(OTF))).*((abs(ratio_f).^beta).*exp(1i*angle(ratio_f)))); % Apply Non-linear reconstruction

    S1 = residue.*S1; % Calculate the next solution

    imagesc(abs(S1).^1); % Display the solution

    pause(0.1) % pause to see the evolution of the solution

end % end for loop

result = abs(S1); % Final solution

imagesc(result) % Display final solution
```

Non-exclusive licence to reproduce the thesis and make the thesis public

I, Oskar Tamm,

1. grant the University of Tartu a free permit (non-exclusive licence) to:

reproduce, for the purpose of preservation, including for adding to the DSpace digital archives until the expiry of the term of copyright, my thesis

Super-resolution correlating optical endoscopy,

supervised by Vijayakumar Anand, PhD, Vipin Tiwari, PhD and Shivasubramanian Gopinath, MSc,

2. I grant the University of Tartu the permit to make the thesis specified in point 1 available to the public via the web environment of the University of Tartu, including via the DSpace digital archives, under the Creative Commons licence CC BY NC ND 4.0, which allows, by giving appropriate credit to the author, to reproduce, distribute the work and communicate it to the public, and prohibits the creation of derivative works and any commercial use of the work from ***dd/mm/yyyy*** until the expiry of the term of copyright,

3. I am aware that the author retains the rights specified in points 1 and 2.

4. I confirm that granting the non-exclusive licence does not infringe other persons' intellectual property rights or rights arising from the personal data protection legislation.

Oskar Tamm

30/05/2024